Batch-to-batch optimization of an industrial reactor using modifier adaptation

Mohamed Aboelnour * **Ala Bouaswaig** * **Sebastian Engell** **

* *BASF SE, 67056 Ludwigshafen, Germany (e-mail: mohamed.aboelnour@basf.com, ala.bouaswaig@basf.com).*
** *Biochemical and Chemical Engineering Department, TU Dortmund, 44221 Dortmund & ZEDO e.V., 44227 Dortmund, Germany (e-mail: sebastian.engell@tu-dortmund.de)*

Abstract: We explore batch-to-batch optimization of a simulated semi-batch process, which represents an important industrial process at BASF. Our primary objectives are to ensure safe batch operations, to produce within specifications, and to increase the throughput. To achieve these goals, Modifier Adaptation with Quadratic Approximation (MAWQA) is employed to optimize key operational parameters iteratively over a sequence of batches. By integrating modifier adaptation with the quadratic approximation used in derivative-free optimization, sensitivity to noise is reduced, and the speed of convergence is improved. A challenging feature of the case considered here is that the constraints involve the maximum temperature and pressure over the batch, which depends on the interaction of feedback controllers with the plant, and that the product quality can only be determined at the end of the batch.

Keywords: Batch to batch optimization, Semi-batch Process, Modifier adaptation.

1. INTRODUCTION

In the industrial process control hierarchy, the real-time optimization (RTO) layer connects the production planning and the control layer. An RTO algorithm computes economically optimal setpoints that are passed to the control layer such that product specifications and plant constraints are met. The successful implementation of RTO algorithms depends strongly on the quality of the model used. To improve the model quality, usually the two-step approach proposed by Jang et al. (1987) is applied. Building and maintaining an accurate process model can be challenging and comes with a significant effort. Roberts (2000) first proposed a combination of model-based and data-based optimization. The proposed Integrated System Optimization and Parameter Estimation (ISOPE) modifies the objective function alongside correcting model parameters. Gao and Engell (2005) suggested modifying the objective function and the constraints iteratively, calling the technique Iterative Gradient-Modification Optimization (IGMO). Marchetti et al. (2009) conducted a detailed analysis of the IGMO approach, referring to it as Modifier Adaptation (MA). MA schemes handle plant-model mismatch by applying bias and gradient corrections to the objective and constraint functions. These corrections are computed from the gradients of the value function and of the constraints of the plant with respect to the optimized variables. Estimating these gradients is a key step in the method. Gao et al. (2016) proposed to use Quadratic Approximation (QA) for process gradient estimation, leading to the development of Modifier Adaptation With Quadratic Approximation (MAWQA). The algorithm fits a surrogate model to measurements of the objective and constraints of the real plant, which reduces the effects of measurement noise while capturing the curvature of the functions.

In this paper an improved version of MAWQA is presented, where a new perturbation method to design plant trials in the case where the available data are not well distributed is employed so that the process optimum is reached faster and more smoothly. Additionally, a stopping criterion based on this new perturbation method is proposed. To demonstrate the performance of the proposed algorithm, we present a process model that replicates an industrial semi-batch production process of high economic relevance to BASF. The behaviour of the model mimics the real plant but some elements are modified for confidentiality reasons. Our focus is on the dosing phase of the batch, as this phase is the most critical and presents significant opportunities for improvement, in particular by reducing the batch time and thus increasing the productivity. The parametric and structural mismatch between the real plant and the available model is represented by using the plant model which is described below as a virtual plant and using a simplified model in the optimization.

2. MODEL OF THE INDUSTRIAL REACTOR

Figure 1 shows a sketch of the reactor with the PI controllers. The reactant, denoted by A, is present in the gas and liquid phases represented by A_g and A_l. The product is referred to as B and the undesired by-product is denoted by D. The batch process goes through the following phases:

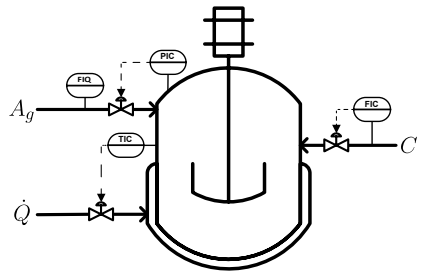

Fig. 1. Semi-batch reactor with control loops.

- **Filling Phase**: The batch begins by filling the reactor with a precharge mass m_O and the catalyst C with mass m_C.
- **Heating Phase**: The reactor is heated to 400K.
- **Dosing Phase**: During this phase, the gaseous reactant A_g is continuously dosed, ensuring a steady supply for the reaction. The temperature is maintained at the reaction temperature setpoint T_{rx} by a PI controller.
- **Post Reaction Phase**: After 30 tonnes of A_g have been dosed, the feeding stops and the reaction continues.
- **Cooling Phase**: Once the reaction has slowed down, the reactor is cooled to 370K.
- **Emptying Phase**: Finally, the reactor content is transferred to the next stages for further processing.

During the batch, the reactor temperature $\tilde{T}_R$, the pressure $\tilde{P}_R$, and the reactant flow $\tilde{F}_A$ are continuously measured. These measurements are corrupted with noise. After the batch ends, samples of the reactor content are collected and the component concentrations are measured in the lab.

Initially, the reactor contains only nitrogen in the gas phase, which is assumed to be present in all batches with the same number of moles, n_{N_2}. The cooling phase begins when the partial pressure of the nitrogen p_{N_2} equals 98% of the measured reactor pressure $\tilde{P}_R$.

$$p_{N_2}(t) := \frac{n_{N_2} \cdot R \cdot \tilde{T}_R}{V_g} > 0.98 \cdot \tilde{P}_R(t), \tag{1}$$

where V_g denotes the volume of the gas phase, and R is the molar gas constant. To avoid the creation of the side product and to facilitate the transfer of the material after the batch has ended, the reactor is cooled down after the dosing is finished and after the mass transfer from the gas to the liquid phase has concluded. The temperature setpoint T_{SP} assumes two values, as described by

$$T_{SP}(t) = \begin{cases} 370, & \text{if (1) holds,} \\ T_{rx}, & \text{otherwise,} \end{cases} \tag{2}$$

where T_{rx} is the temperature setpoint in the dosing phase, which is an output of the RTO scheme. All parameters are listed in table 1.

2.1 Control loops

For this reactor, two control loops are important. The first loop controls the reactor pressure by manipulating the feed rate of the reactant A. This structure was chosen because the pressure reflects the reactant hold-up within the reactor. The setpoint P_{SP} is set to 19.6bar to ensure a safe operation below the pressure safety constraint of 20bar. The pressure controller has a gain and an integral time denoted by $\mathcal{K}_P$, $\mathcal{T}_P$. The maximum permissible feed is denoted by $\bar{F}_A$. The feed enters the reactor at a temperature T_{F_A}. The energy added to the system through F_A, denoted by $\dot{Q}_{F_A}$, is computed by

$$\dot{Q}_{F_A} = c_{p,A_g} \cdot F_A \cdot (T_{F_A} - T_R)\,, \tag{3}$$

where c_{p,A_g} denotes the specific heat capacity of A_g.

The second control loop controls the reactor temperature. For simplicity, the dynamics of the jacket are not explicitly modeled. Instead, the input power $\dot{Q}$ is used as a manipulated input, considering the available cooling and heating powers that are bounded by the limits $\dot{Q}_l$ and $\dot{Q}_h$. The heat flow is set by a PI controller, which aims to track T_{SP} in (2). The temperature controller gain and integral time are denoted by $\mathcal{K}_T$ and $\mathcal{T}_T$.

Table 1. Parameters of the virtual plant

Name	Value [Unit]	Name	Value [Unit]
m_O	20[t]	n_{N_2}	900[mol]
R	8.314[J/mol/K]	T_S	15[s]
$\mathcal{K}_T$	0.002	$\mathcal{T}_T$	1000
$\mathcal{K}_P$	0.05	$\mathcal{T}_P$	180
$\bar{F}_A$	20[t/h]	T_{F_A}	283.15[K]
$\dot{Q}_l$	−5000[kW]	$\dot{Q}_h$	5000[kW]
ρ_{A_l}	700[kg/m^3]	ρ_B	1400[kg/m^3]
ρ_C	1000[kg/m^3]	ρ_D	1400[kg/m^3]
ρ_O	1000[kg/m^3]	V_R	50[m^3]
$c_{p,A}$	3.8[kJ/kg/K]	c_{p,A_g}	1.0[kJ/kg/K]
$c_{p,B}$	2.1[kJ/kg/K]	$c_{p,C}$	0.93[kJ/kg/K]
$c_{p,D}$	4.0[kJ/kg/K]	$c_{p,O}$	2.5[kJ/kg/K]
c_{p,N_2}	1.0[kJ/kg/K]	m_{N_2}	25.2[kg]
k_{1o}	260[m^3/s/mol]	E_1	6000[K]
k_{2o}	$2.835 \cdot 10^{-13}$[m^9/s/mol^3]	E_2	800[K]
k_{3o}	3.5[m^3/s/mol]	E_3	7000[K]
ΔH_1	−60[kJ/mol]	ΔH_2	−70[kJ/mol]
ΔH_3	−250[kJ/mol]	An	8.6941[-]
Bn	266.8665[K]	Cn	−215.8753[K]
k_{sp0}	−2.59[-]	k_{sp}^B	0.15[-]
k_{sp}^T	0.007[1/K]	k_{VLE}	0.006[-]
MW_A	50[g/mol]	MW_B	50[g/mol]
MW_C	200[g/mol]	MW_D	150[g/mol]
$\hat{k}_{1o}$	453[m^3/s/mol]	$\hat{E}_1$	6150[K]
$\hat{k}_{2o}$	$1.71 \cdot 10^{-12}$[m^9/s/mol^3]	$\hat{E}_2$	1300[K]
$\Delta\hat{H}_1$	−50[kJ/mol]	$\Delta\hat{H}_2$	−490[kJ/mol]
$\hat{k}_{sp0}$	0.42[-]		

2.2 Physical properties

The temperature of the gas and liquid phases are assumed equal. It is also assumed that N_2 and A_g behave as ideal gases, hence their partial pressures can be computed from the ideal gas law: $p_i V_g = n_i R T_R$. Therefore, the reactor pressure results as $P_R = p_{N_2} + p_{A_g}$. The volume of the gas phase $V_g = V_R - V_l$ is computed from $V_l = \sum_i \frac{m_i}{\rho_i}, \quad \forall i \in \{A_l, B, C, D, O\}$ where V_l is the volume of the liquid phase, and V_R is the total volume of the reactor. The masses of the components are denoted by m_i, where the subscript indicates the component. Similarly the densities are denoted by ρ_i. The total mass in the liquid phase is denoted by $M_l := \sum_i m_i, \quad \forall i \in \{A_l, B, C, D, O\}$. The heat capacity of the reactor content, denoted as C_p, is calculated by $C_p = \sum_i m_i \cdot c_{p,i}, \quad i \in \{A_l, A_g, B, C, D, N_2, O\}$ where $c_{p,i}$ denotes the specific heat capacity.

2.3 Virtual plant

In this subsection, the virtual plant dynamics is introduced, which results from the following reaction mechanism:

$$A_l \xrightarrow{k_1} B \qquad A_l + 2B \xrightarrow{k_2} D \qquad B \xrightarrow{k_3} \frac{1}{3}D,$$

The reaction rate constants k_i depend on the reactor temperature according to the Arrhenius law

$$k_i = k_{io} \cdot e^{-\frac{E_i}{T_R}}, \quad i \in [1,3]. \tag{4}$$

The reaction rates are calculated by considering the molar concentrations of the components, denoted by c_i, and the corresponding reaction rate constants, as shown in (5).

$$c_i = \frac{m_i}{MW_i \cdot V_l}, \qquad r_1 = k_1 \cdot c_{A_l} \cdot c_C, \tag{5a}$$

$$r_2 = k_2 \cdot c_{A_l} \cdot c_B^2 \cdot c_C \cdot X_B, \qquad r_3 = k_3 \cdot c_B \cdot c_C, \tag{5b}$$

where MW_i denotes the molar weight of the components and $X_B := \frac{m_B}{M_l}$ refers to the mass fraction of B. The reactions are exothermic, and the total heat of reaction $\dot{Q}_r = \sum_{i=1}^{3} -r_i \cdot V_l \cdot \Delta H_i$. The liquid-vapor equilibrium of the reactant A is computed from its solubility in the product-precharge mixture and the equilibrium pressure of A in the gas phase. First the equilibrium pressure is calculated from the Antoine equation $\log_{10} p_A^{eq} = A_n - \frac{B_n}{C_n + T_R}$. The solubility of A is a function of the reactor temperature and of X_B as described by $k_{sp} = k_{sp0} + k_{sp}^T \cdot T_R + k_{sp}^B \cdot X_B$. Finally, the mass transfer rate is computed from (6).

$$q_A = k_{VLE}(k_{sp} \cdot \frac{p_{A_g}}{p_A^{eq}} - \frac{m_{A_l}}{M_l}). \tag{6}$$

The states are the masses in kg of the components; $m_{A_g}, m_{A_l}, m_B, m_D$ and the reactor temperature T_R in K. The effects of condensation and vaporization in the energy balance is neglected. The resulting dynamic equations that describe the virtual plant are shown in (7).

$$\frac{dm_{A_g}}{dt} = F_A - q_A \cdot M_l, \tag{7a}$$

$$\frac{dm_{A_l}}{dt} = q_A \cdot M_l - (r_1 + r_2) \cdot V_l \cdot MW_A, \tag{7b}$$

$$\frac{dm_B}{dt} = (r_1 - 2r_2 - r_3) \cdot V_l \cdot MW_B, \tag{7c}$$

$$\frac{dm_D}{dt} = (r_2 + \frac{1}{3}r_3) \cdot V_l \cdot MW_D, \tag{7d}$$

$$C_p \cdot \frac{dT_R}{dt} = \dot{Q} + \dot{Q}_r + \dot{Q}_{F_A}. \tag{7e}$$

2.4 Optimization model

It is assumed that the reaction scheme of the plant is not well understood. The third reaction does not exist in the optimizer model, i.e. $\hat{r}_3 := 0$. The notation $\hat{(\cdot)}$ denotes quantities related to the optimization model. The reaction rate constants of the optimization model with the corresponding reaction rates are

$$\hat{k}_i = \hat{k}_{io} \cdot e^{-\frac{\hat{E}_i}{T_R}}, \qquad i \in [1,2], \tag{8a}$$

$$\hat{r}_1 = \hat{k}_1 \cdot c_{A_l} \cdot c_C, \qquad \hat{r}_2 = \hat{k}_2 \cdot c_{A_l} \cdot c_B^2 \cdot c_C. \tag{8b}$$

Since only two reactions are assumed in the optimization model, the heat of reaction is computed by $\hat{\dot{Q}}_r = \sum_{i=1}^{2} -\hat{r}_i \cdot V_l \cdot \Delta \hat{H}_i$. In addition, the solubility is assumed to be constant in the optimization model, which yields the mass transfer rate

$$\hat{q}_A = k_{VLE}\left(\hat{k}_{sp0} \cdot \frac{p_{A_g}}{p_A^{eq}} - \frac{m_{A_l}}{M_l}\right). \tag{9}$$

The parameters of the optimization model were fitted to simulations of the virtual plant at $T_{rx} = 430$K, and $m_C = 60$kg. This operating point is safe and meets the required specifications. Continuous measurements during the batch and the lab measurements taken after the end of the batch were used to fit the model parameters as it is done in industrial practice. Table 1 contains the fitted parameters of the optimization model. The dynamic equations of the optimization model are given below.

$$\frac{dm_{A_g}}{dt} = F_A - \hat{q}_A \cdot M_l, \tag{10a}$$

$$\frac{dm_{A_l}}{dt} = \hat{q}_A \cdot M_l - (\hat{r}_1 + \hat{r}_2) \cdot V_l \cdot MW_A, \tag{10b}$$

$$\frac{dm_B}{dt} = (\hat{r}_1 - 2\hat{r}_2) \cdot V_l \cdot MW_B, \tag{10c}$$

$$\frac{dm_D}{dt} = \hat{r}_2 \cdot V_l \cdot MW_D, \tag{10d}$$

$$C_p \cdot \frac{dT_R}{dt} = \dot{Q} + \hat{\dot{Q}}_r + \dot{Q}_{F_A}. \tag{10e}$$

Figure 2 shows a comparison of the behaviour of the virtual plant and of the optimization model. Despite the structural mismatch, the first part of the batch is described with good accuracy. However, the decaying pressure is not reproduced perfectly. The optimization model was fitted with a focus on accurately capturing both the profit function and the constraints. This precision is crucial for MA algorithms, as noted by Srinivasan and Bonvin (2019).

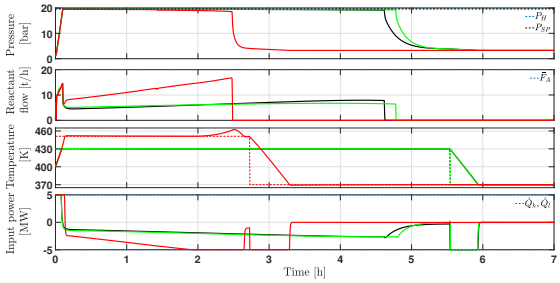

Fig. 2. Batch trajectories of the virtual plant (in black) and of the optimization model (in green) for $T_{rx} = 430$K, and $m_C = 60$kg and the optimum batch run shown in red for $T_{rx} = 451.1$K, and $m_C = 94.6$kg.

2.5 Batch-to-batch optimization

The main goal of the application of batch-to-batch optimization is to increase the capacity of the plant by producing in-spec products as fast as possible. However, achieving this objective may result in increased usage of cooling and heating power, as well as an increased amount of the catalyst, which is assumed to be expensive. The product must meet the required specifications, specifically the mass fraction of component D must be kept below 5%. There

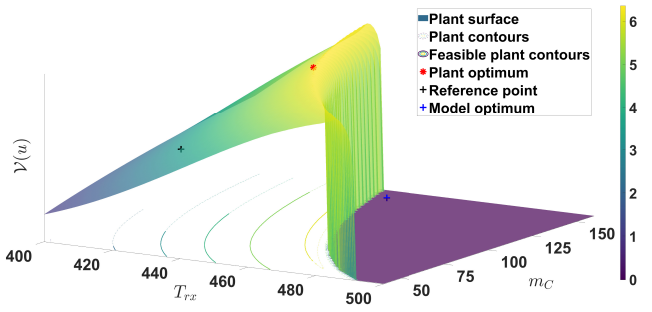

Fig. 3. Surface plot of the noise-free profit function.

are critical temperature and pressure limits that have to be respected to avoid any potential thermal runaway. The high-pressure limit is set at 20bar. The maximum tolerated temperature is a function of the specified reaction temperature setpoint, i.e., $T_H = T_{rx} \times 1.05$. However, the optimization uses a conservative back off from the limit T_H as shown in (11c). The degrees of freedom, denoted by u, are the setpoint of the reaction temperature T_{rx} and the mass of catalyst m_C, which is dosed at the beginning of the batch. The optimization problem is formalized in (11), which specifies the profit function, constraints:

$$\max_{T_{rx},m_C} \mathcal{V}(u) := \frac{3m_B(t_f) - 0.4\mathcal{E} - 50m_C}{t_f}, \tag{11a}$$

$$\text{s.t.} \quad X_D(t_f) \leq 0.05, \tag{11b}$$

$$\tilde{T}_R(t) < T_{rx} \times 1.025, \quad \tilde{P}_R(t) < P_Z^+, \tag{11c}$$

$$T_{rx} \in [400, 500], \qquad m_C \in [50, 150], \tag{11d}$$

where t_f represents the time from the start of dosing until the reactor is ready for emptying. This occurs when 30 tonnes of A have been dosed and the reactor temperature has been cooled down to $373K$. Equation (12) formalizes the definition of t_f.

$$t_f := \min t \mid T_R(t) \leq 373 \, , \int_0^t F_A(\tau)d\tau \geq 3 \times 10^4. \tag{12}$$

The energy consumption during the batch, denoted as $\mathcal{E}$ is computed by integrating $\dot{Q}$ and is computed in kWh. Whether the constraints defined in (11c) are met depends on the performance of the temperature and pressure PI controllers and the chosen values of u. The fact that the product amount m_B and the side product mass fraction X_D can only be measured after the batch has been finished motivated the application of batch-to-batch optimization. The input power $\dot{Q}$ and the dosing profile F_A are determined through the actions of the PI controllers. The surface of the profit function $\mathcal{V}$, without measurement noise, is depicted in figure 3. The range of feasible operation is represented by solid contour lines. Although the fitted parameters represent the virtual plant well at the reference point, the optimum that results when employing the optimization model leads to off-spec product and an unsafe operation. The optimum depends on the tuning of the PI controllers and time discretization.

3. THE IMPROVED MAWQA ALGORITHM

In Modifier Adaptation, the optimization problem is adapted with modifiers to ensure that the KKT conditions of the plant are satisfied upon convergence. The adapted inputs $u_{ad,k}$ in the k^{th} iteration are computed from (13).

$$u_{ad,k} := \arg\max_u \left(\hat{\mathcal{V}}(u) + \epsilon_k^{\mathcal{V}} + (\psi_k^{\mathcal{V}})^T (u - u_k) \right), \tag{13a}$$

$$\text{s.t.} \quad \hat{G}(u) + \epsilon_k^G + (\psi_k^G)^T (u - u_k) \leq 0, \tag{13b}$$

where $\hat{\mathcal{V}}(u)$ represents the profit function which is computed using the optimization model. Similarly $\hat{G}(u)$ denotes the constraints that are evaluated using the optimization model. The measured process objective and constraints are denoted by $\tilde{\mathcal{V}}(u_k)$ and $\tilde{G}(u_k)$. To reduce the effect of errors in the estimation of the gradients of the real plant, the inputs can be filtered according to

$$u^*_{ad,k+1} = K \cdot u_{ad,k+1} + (I - K) \cdot u^*_{ad,k}, \tag{14}$$

where K is a gain matrix (Marchetti et al., 2009).

A challenge in MA lies in accurately estimating the plant gradients online, particularly when dealing with noisy measurements.

3.1 Modifier adaptation with quadratic approximation

In MAWQA, it is proposed to estimate the gradients based on quadratic surrogate models that are fitted to the data that was collected at the previous data points. A minimum number $p = \frac{(n_u+1)(n_u+2)}{2}$ of measurements is needed, where n_u is the dimension of u. The choice of the regression set, denoted here as $\mathcal{U}_k \subseteq \mathbb{U}_k$, where $\mathbb{U}_k$ is the set with all data points, plays an important role in the quality of the fitted model as discussed in Conn et al. (2009). The regression set is identified by screening all the available data points in $\mathbb{U}_k$. Generally $\mathcal{U}_k$ should consist of well-distributed distant data points, denoted as $\mathcal{U}_{k,\text{dist}}$, which serve as anchor points and all neighboring points near the current best iterate u^*_k, denoted as $\mathcal{U}_{k,\text{nb}}$ with $\|u - u^*_k\| \leq \delta_k$ for all $u \in \mathbb{U}_k$. Model adequacy can be considered while fitting the quadratic model by the method proposed by Gottu Mukkula and Engell (2020), where the Hessian matrix of the fitted surrogate model is forced to be positive semi-definite. The fitted functions are denoted by $\mathcal{V}_\phi(u)$ and $G_\phi(u)$. As the fitted model is only a local approximation of the original function around the point u^*_k, a trust region is defined while searching for u_{k+1}. The trust region is computed from the inverse of the covariance matrix of the regression set, denoted by $\text{cov}(\mathcal{U}_k)$.

$$u^*_{\phi,k+1} := \arg\min_u \mathcal{V}_\phi(u) \tag{15a}$$

$$\text{s.t.} \quad G_\phi(u) \leq 0 \tag{15b}$$

$$(u - u_k)^T \, \text{cov}(\mathcal{U}_k)(u - u_k) \leq \gamma^2, \tag{15c}$$

where γ is a tuning factor used to enlarge or shrink the trust region. To monitor the quality of the surrogate model compared to the known optimization process model a quality check step is performed as described in Gao et al. (2016) to determine whether the modified optimization problem (13) is solved or the optimization is performed using the quadratic approximation (15).

3.2 The improved MAWQA algorithm

In this paper, the MAWQA algorithm is enhanced by integrating a perturbation method and proposing a new stopping criterion. As shown by Conn et al. (2009), the condition number is closely related to the so-called Λ

poisedness. We here utilize this measure of well-poisedness as the basis of a new perturbation method. The algorithm improves the distribution of the available data points in the input space using an adapted version of a method proposed by Conn et al. (2009). The goal is to obtain test inputs u_{tp} that improve the $\Lambda-$poisedness of $\mathcal{U}_k$, while respecting the constraints of the optimization problem. The basis of Lagrange polynomials, denoted by $\ell(\cdot)$, of the p best distributed points in $\mathcal{U}_k$. A set $\mathcal{U}_k$ is called Λ-poised in a ball with radius Δ if and only if $\Lambda \geq \max_{1<i<p} \max_{u\in\Delta} |\ell_i(u)|$ for the corresponding basis of Lagrange polynomials. Algorithm 1 computes trial points $u_{tp,i}$ such that the regression set becomes at least $\bar{\Lambda}$ poised. One can compute only one trial point at a time or find all trial points and then define a criterion for selecting the best one. Different criteria can be chosen, such as: the furthest point from u_k^* or the point that would give the best value of Λ. The algorithm starts by computing the Lagrange polynomials for the first p points in $\mathcal{U}_k$, which is assumed to be $\{u_k^*\} \cup \mathcal{U}_{k,\text{dist}}$. It then improves the point distribution to enhance the $\Lambda-$poisedness of the setpoints, while respecting the constraints. Due to the constraints (16b), it may not be possible to reach the desired value of $\bar{\Lambda}$, instead the algorithm computes points that yield the best feasible value. u_{tp} is searched for in a ball of radius Δ_k around the current optimum u_k^*. A simple choice is $\Delta_k = \delta_k$. The best achievable poisedness value is $\Lambda = 1$.

Algorithm 1 Surrogate Model Improvement

Require: $\mathcal{U}_k$, which has u_k^* as the first entry, the desired well poisedness value denoted by $\bar{\Lambda}$, and a radius Δ_k
Start: Compute $\ell_i(u)$ for $\{u_k^*\} \cup \mathcal{U}_{k,\text{dist}}$.
Improve point distribution
for $i \in \{1, ..., p\}$ **do**
  if $\max_{u\in\Delta_k} |\ell_i(u)| > \bar{\Lambda}$ **OR** $i = p$ **then**

$$u_{tp,i} = \arg\max_u |\ell_i(u)| \tag{16a}$$

$$\text{s.t. } G_\phi(u) \leq 0 \tag{16b}$$

$$\|u - u_k^*\| < \Delta_k, \tag{16c}$$

  if $u_{tp,i} \notin \mathbb{U}_k$ **return** $u_{k+1} = u_{tp,i}$.
end for

The improved MAWQA algorithm is initiated with p data points. If $\mathcal{U}_k$ is not well poised or if p points are not available, $\mathcal{U}_k$ is completed using algorithm 1. Another improvement over the original MAWQA is that if the calculated input is close to u_k^*, a trial input computed by algorithm 1 is applied then the search space Δ_k as well as δ_k, which is used for constructing $\mathcal{U}_k$, are reduced. The plant trials are computed to reach the specified poisedness $\bar{\Lambda}$ or until it cannot be improved further. The search radius is reduced until it reaches a termination threshold ϵ, signaling convergence.

4. RESULTS

In this section, the results of applying the improved MAWQA algorithm to the case study introduced in section 2 is presented. The starting point is the reference point of $u_0 := [430, 60]$. From this starting point, two perturbations are executed, with step sizes of +10K and +10kg. The first p points required to start algorithm 2 are generated using (13) with (14). For these steps, the condition number of the

Algorithm 2 Improved MAWQA

Require: p well poised points with u_0^* as the current best iterate, set $k = 0$, and choose values for $\bar{\Lambda}, \Delta_k,$ and δ_k.
repeat
Step 1. Construct $\mathcal{U}_k$ as outlined by Gao et al. (2016).
Step 2. Compute the next input u_{k+1} after applying the quality check from Gao et al. (2016) to compute u_{k+1} from (13) or (15).
If $\|u_k^* - u_{k+1}\| > \delta_k/2$, go to **Step 4.**
Step 3. Apply algorithm 1 to get a different value of u_{k+1} and set $\delta_k = \delta_k/2, \Delta_k = \Delta_k/2$.
Step 4. Apply the input u_{k+1} to the plant.
Step 5. Measure $\tilde{\mathcal{V}}(u_{k+1})$ and $\tilde{G}(u_{k+1})$ and set

$$u_{k+1}^* = \begin{cases} u_{k+1}, & \tilde{G}(u_{k+1}) \leq 0, \tilde{\mathcal{V}}(u_{k+1}) > \tilde{\mathcal{V}}(u_k^*) \\ u_k^*, & \text{otherwise.} \end{cases} \tag{17}$$

Step 6. Set $k = k + 1$
until $\Delta_k \leq \epsilon$

previous set of inputs is monitored. If $\text{cond}^{-1}(\mathcal{U}_k) < 0.2$ or if $\|u_k^* - u_{ad,k+1}^*\| < \delta_k/2$, algorithm 1 is applied to compute a geometry improving input. This replaces the optimization of the condition number in IGMO.

The profit function $\mathcal{V}(u)$ is corrupted with measurement noise of ± 0.05. Lab measurement of X_D has an accuracy of 0.1%. The pressure and temperature sensor accuracies are ± 0.02bar and ± 0.1K. All measurement errors are assumed to be uniformly distributed within these limits. Measurement noise in the temperature and pressure readings influences the actions of the PI controllers during the batch, introducing stochastic behavior that disturbs the RTO algorithm. When the optimization starts at $t = 0$, the reactor is already filled with the precharge m_O and the specified catalyst amount m_C, and heated to a temperature of 400K. The initial state vector is $x_0 := [0, 0, 0, 0, 400]$.

Table 2. Tuning parameters of the improved MAWQA algorithm for the batch case study

$\gamma = 0.2$	$K = 0.15$	$\delta_0 = 0.05$	$\Delta_0 = 0.05$	$\epsilon = 0.01$	$\bar{\Lambda} = 5$

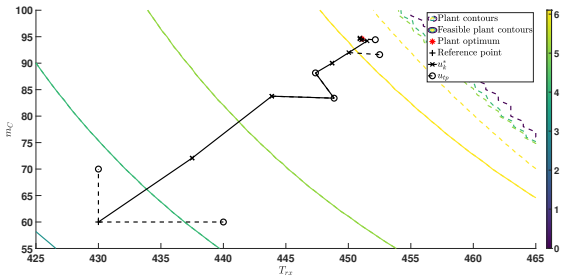

Fig. 4. Result of applying the improved MAWQA algorithm to the semi-batch process. Successful iterations are depicted by solid lines marked with **x**, while the trial points are marked with **o** and dashed lines.

As illustrated in figure 4, the iterations of the inputs succeed in identifying the plant optimum while respecting the constraints along the trajectory. The vicinity of the virtual plant optimum is reached within 10 steps. The algorithm was able to determine good plant trials that improve the accuracy of the fitted surrogate models. In figure 2 the trajectories for the optimal parameters are shown together

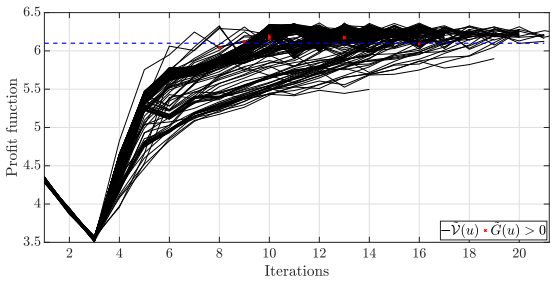

Fig. 5. Extensive simulation of the improved MAWQA algorithm. The black lines represents the optimal values achieved at each iteration. The red crosses indicate slight violation of the constraints.

with those of the reference batch. The optimum batch is completed faster than the reference batch while also meeting the safety limits and product specifications, with $X_D = 4.22\%$ at the end of the optimum batch run. Notably, utilizing this software solution significantly improves the performance of the system even though the starting point is far away from the reference; such as the one used in this simulation run u_0. For the optimized batch, the temperature controller does not track the temperature setpoint tightly. Therefore the RTO scheme has to cope with a point-wise active constraint. This issue can be attributed to the inherent limitations of the PI controllers. In the setup considered here, the feed rate results from the controlled pressure, neglecting the influence on the temperature. Ideally, the feed should be slowed down when T_{SP} cannot be met due to cooling power limitations. A single PI controller cannot adequately handle this task. The RTO scheme considers these limitations of the SISO PI controllers. Several key performance indicators (KPIs) were computed to evaluate the algorithm:

(1) **Optimum Proximity KPI**: This KPI assesses whether the point of convergence is near the optimum of the virtual plant, which has a value of 6.25. The vicinity is defined as reaching a final value ≥ 6.1.
(2) **Average steps KPI**: This indicator provides the average number of iterations needed to approach the vicinity of the optimum, if it is reached.
(3) **Violation KPI**: This KPI quantifies the percentage of iterations that violate the constraints.
(4) **Convergence KPI**: This KPI indicates the average number of iterations needed until the stopping criterion of algorithm 2 is met.

A total of 200 simulation runs were performed with the same initial point while varying only the noise. All simulations were conducted twice, using the proposed algorithm and the original MAWQA algorithm. Table 3 summarizes the results for the KPIs defined above. The values of the original MAWQA algorithm are shown in parentheses. The execution time for algorithm 2 is orders of magnitude less than the time required to simulate a single batch.

Table 3. Results of the improved MAWQA.

Optimum Proximity 99% (87%)	Average steps 11.3 (18.2)
Violation 0.25% (0.11%)	Convergence 16.1

Despite the plant-model mismatch, the true optimum was successfully identified. The stopping criterion enabled the algorithm to terminate within the first 22 iterations, with a minimum of 10 including all perturbation steps as depicted in figure 5. The remaining 1% that did not converge to the optimum was due to measurement noise, which caused early convergence of the algorithm. Navigating near the optimum was particularly challenging due to the presence of a flat surface in that region as depicted in figure 3. The measurement noise significantly impacted the first p points, which contributed to a slower convergence rate in some instances. The tuning parameters were chosen such that only small steps are performed, resulting in an average of 11 steps to reach the neighborhood of the optimum. While more aggressive steps could be performed to accelerate the convergence this leads to constraint violations of T_H due to the limitations of SISO PI controllers.

5. CONCLUSION

We presented a model of an industrial case study for batch-to-batch optimization and an improved version of the MAWQA algorithm for optimization. The goal is to increase the capacity of the plant by adjusting the reaction temperature setpoint and the amount of catalyst used. The improved version of MAWQA incorporates a novel perturbation strategy, which led to the establishment of a stopping criterion. Despite using a structurally incorrect model, the algorithm was able to find the correct process optimum in 99% of the cases. The instances with early convergence require further investigations. Since p increases quadratically with n_u, the proposed method proves practical up to $n_u = 5$. It is recommended to implement a multi-variable control e.g. NMPC to expand the feasible domain, potentially leading to greater productivity gains.

REFERENCES

Conn, A.R., Scheinberg, K., and Vicente, L.N. (2009). *Introduction to Derivative-Free Optimization*. Society for Industrial and Applied Mathematics, USA.

Gao, W. and Engell, S. (2005). Iterative set-point optimization of batch chromatography. *Computers & Chemical Engineering*, 29, 1401–1409.

Gao, W., Wenzel, S., and Engell, S. (2016). A reliable modifier-adaptation strategy for real-time optimization. *Computers & Chemical Engineering*, 91, 318–328.

Gottu Mukkula, A.R. and Engell, S. (2020). Guaranteed model adequacy for modifier adaptation with quadratic approximation. *2020 European Control Conference (ECC)*, 1037–1042.

Jang, S.S., Joseph, B., and Mukai, H. (1987). On-line optimization of constrained multivariable chemical processes. *AIChE Journal*, 33, 26–35.

Marchetti, A., Chachuat, B., and Bonvin, D. (2009). Modifier-adaptation methodology for real-time optimization. *Industrial & Engineering Chemistry Research*, 48, 6022–6033.

Roberts, P. (2000). Broyden derivative approximation in ISOPE optimising and optimal control algorithms. *IFAC Proceedings Volumes*, 33, 293–298.

Srinivasan, B. and Bonvin, D. (2019). A feature-based analysis of static real-time optimization schemes. *Industrial & Engineering Chemistry Research*, 58, 14227–14238.